# ARTICLE

# Porous materials with pre-designed single-molecule traps for $CO_2$ selective adsorption

Jian-Rong Li[1,2], Jiamei Yu[3,4], Weigang Lu[2], Lin-Bing Sun[2], Julian Sculley[2], Perla B. Balbuena[3,4] & Hong-Cai Zhou[2,3]

Despite tremendous efforts, precise control in the synthesis of porous materials with pre-designed pore properties for desired applications remains challenging. Newly emerged porous metal-organic materials, such as metal-organic polyhedra and metal-organic frameworks, are amenable to design and property tuning, enabling precise control of functionality by accurate design of structures at the molecular level. Here we propose and validate, both experimentally and computationally, a precisely designed cavity, termed a 'single-molecule trap', with the desired size and properties suitable for trapping target $CO_2$ molecules. Such a single-molecule trap can strengthen $CO_2$–host interactions without evoking chemical bonding, thus showing potential for $CO_2$ capture. Molecular single-molecule traps in the form of metal-organic polyhedra are designed, synthesised and tested for selective adsorption of $CO_2$ over $N_2$ and $CH_4$, demonstrating the trapping effect. Building these pre-designed single-molecule traps into extended frameworks yields metal-organic frameworks with efficient mass transfer, whereas the $CO_2$ selective adsorption nature of single-molecule traps is preserved.

[1] College of Environmental and Energy Engineering, Beijing University of Technology, Beijing 100124, China. [2] Department of Chemistry, Texas A&M University, College Station, Texas 77842, USA. [3] Materials Science and Engineering Program, Texas A&M University, College Station, Texas 77842, USA. [4] Department of Chemical Engineering, Texas A&M University, College Station, Texas 77842, USA. Correspondence and requests for materials should be addressed to H.-C.Z. (email: zhou@chem.tamu.edu).

Gas separation and purification are ongoing research topics, attracting interest from both academia and industry. In the last few years, $CO_2$ separation, as a key component of carbon capture, utilisation and storage, has become a fast-growing research area. Carbon capture, utilisation and storage may provide a temporary solution for the continued use of fossil fuels until renewable energy becomes abundant, alleviating the emission of anthropogenic greenhouse gases[1,2]. Two important clean-energy-related separations involving $CO_2$ are $CO_2$ capture from flue-gas streams of power plants, and natural-gas upgrading. The first entails separating $CO_2$ and $N_2$, often under the harsh conditions of flue-gas streams from fossil-fuel-fired power plants. In natural-gas upgrading, from both natural reservoirs and landfills, the separation of $CO_2$ from $CH_4$ improves $CH_4$ purity and reduces pipeline corrosion by the acidic $CO_2$ gas. Various technologies for $CO_2$ capture/separation from its mixture with other gases have been developed, including the relatively mature amine-scrubbing procedure[3], and other techniques that are under intense exploration. Among them, adsorptive and membrane-based separations are some of the most promising because of their potential for simple and low-energy-consumption processes. The performance of porous materials, the supporting medium of adsorbent and membrane, is critical for efficient separation. Many porous solids such as zeolites and activated carbons have been widely studied for clean-energy-related separations, including $CO_2$ capture[4]. However, methods for precise structural and property control of these materials, particularly at the molecular level, are still lacking. Recently, remarkable progress has been made in this regard in the development of metal-organic materials (MOMs), such as metal-organic frameworks (MOFs)[5,6] and metal-organic polyhedra (MOPs)[7], assembled from molecular building units. These materials possess unique properties and vast application potential[8–24]. The hallmark of these new materials is their modular design, which is far beyond the scope of other porous materials[22,25–36] and allows for facile structure and property tuning. This therefore enables precise control of functions by accurate design of structures at the molecular level.

Although many MOFs have been prepared for $CO_2$ separation in recent years, a precise construction implemented at the true molecular level is rare. Herein, as an experimental proof-of-concept, we demonstrate how it is possible to design a cavity specifically for the capture of a single $CO_2$ molecule. The first step is the design and synthesis of a molecular cavity, designated 'single-molecule trap' (SMT) for the convenience of discussion, starting from the evaluation of the size and properties of the guest $CO_2$ molecule (Fig. 1a). As molecular building blocks, these SMTs can be linked to construct a three-dimensional (3D) MOF to ensure efficient transport of $CO_2$ in and out of the cavities. An alternative route is the impregnation of an existing porous material such as mesoporous silica with SMTs directly (Fig 1b). In both cases, the selectivity of the SMT for $CO_2$ should be preserved.

A $CO_2$ molecule is linear, about 2.4 Å long, positively charged at the C atom, and negatively charged at the O atoms. The normal M–O co-ordination bond length, where M represents a transition metal, is about 2.0–2.8 Å. Derived from the above distances, two positively charged 'anchors'[13] separated by about 6.4–8.0 Å ($2.4 + 2 \times$ M–O) distance would be ideal for holding a $CO_2$ molecule between them through electrostatic interactions. Negatively charged groups surrounding the C atom should strengthen the $CO_2$–trap interaction even further. With these considerations in mind, we have prepared a molecular cage using four bridging ligands and two metal clusters (with open metal sites), which are separated by about 7.4 Å (from crystal structural determination) and expected to form strong electrostatic interactions with the negative O atoms of $CO_2$, without the formation of a chemical bond. Such precisely designed SMTs should hold one $CO_2$ molecule per cavity, excluding other small molecules such as $N_2$ and $CH_4$, allowing for the highly selective adsorption of $CO_2$ over other gases. Herein, we describe the design and synthesis of such functional porous materials for efficient $CO_2$ molecule capture, as well as the evaluation of the resulting materials by both molecular simulations and experiments. This exemplifies a new strategy in the highly controllable design and preparation of porous materials for specific adsorption-related applications.
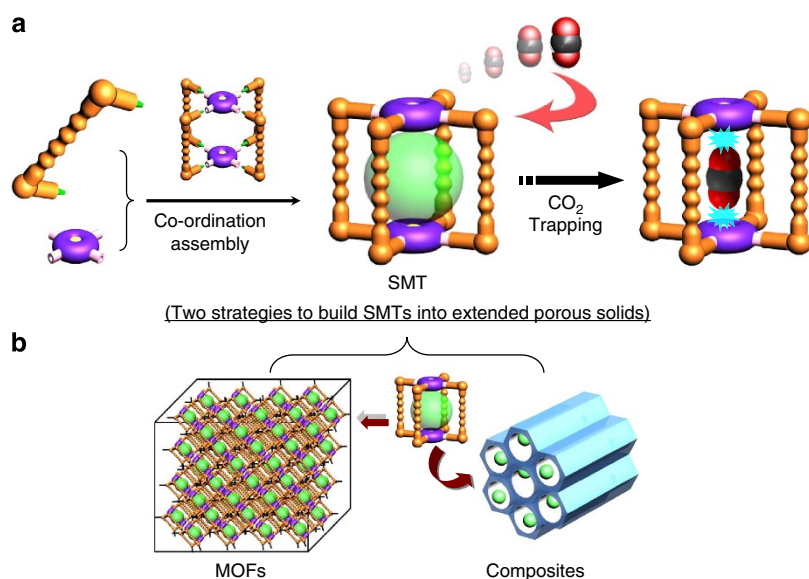


**Figure 1 | Designing porous materials with SMTs for $CO_2$ molecule capture.** (**a**) Schematic representation of the design and construction of a SMT for $CO_2$ adsorption. Organic linker is shown in orange, and the metal node with an open adsorption site is shown in purple and yellow; green spheres represent the cavity for $CO_2$ adsorption. (**b**) Two proposed strategies for building a pre-designed SMT into extended porous solids: assembly of the SMTs by ligand extension and accommodation of SMTs into other porous materials, such as mesoporous silica.

## Results

**MOP-based SMTs for CO$_2$ selective adsorption.** To construct a MOP with fixed shape and distance between metal atoms, an organic ligand with appropriate geometry and size is a prerequisite. Our recent success in the assembly of MOPs with a variety of shapes, sizes and functional groups, by tuning the bridging ligands, enables us to synthesise a single cavity specifically designed for the accommodation of one CO$_2$ molecule[7,37]. In this work, two dicarboxylic acid ligands, 3,3′-(naphthalene-2,7-diyl)dibenzoic acid (H$_2$L$^1$) and 3,3′-(1,8-naphthyridine-2,7-diyl)dibenzoic acid (H$_2$L$^2$) were designed and synthesised by Pd-catalysed coupling reactions between 3-(methoxycarbonylphenyl)boronic acid and 2,7-dibromonaphthalene or 2,7-dibromo-1,8-naphthyridine, respectively, followed by hydrolysis of the corresponding esters. With the 'cis and parallel' arrangement of the two carboxylic acid groups in each ligand, both have a bridging angle of 0° and an inter-carboxylic-acid distance of about 7 Å, thus fulfilling both metal–metal distance and anchor orientation requirements in the resulting MOPs. The SMTs were assembled from H$_2$L$^1$ and H$_2$L$^2$, shown in Fig. 2a, by reacting with Cu$_2$(OAc)$_4$·2H$_2$O in *N,N*-dimethylacetamide (DMA) to give isostructural [Cu$_2$(L$^1$)$_2$(DMA)$_2$]$_2$ (**SMT-1**-DMA) and [Cu$_2$(L$^2$)$_2$(DMA)$_2$]$_2$ (**SMT-2**-DMA), at room temperature as

phase-pure crystals, confirmed by a good match between the experimental and simulated powder X-ray diffraction (PXRD) patterns (Supplementary Figs S1 and S2).

The structures of the two compounds were determined by single crystal X-ray diffraction. As expected, both MOP molecules have a lantern-type structural arrangement with four bridging ligands surrounding two paddlewheel dicopper motifs to form a large paddlewheel tetragonal cage (Fig. 2b and Supplementary Figs S13 and S14). Each copper atom is coordinated by four carboxylate oxygen atoms of different ligands in the equatorial positions and one DMA molecule in the axial position, which can be removed to leave an open metal site. The dimensions of the two MOPs excluding coordinated solvents in height (Cu–Cu) and diameter (C–C between two opposite ligands) are 12.6 × 19.4 and 11.9 × 19.8 Å, respectively; and the inner cavity sizes are 7.4 × 10.7 and 6.7 × 12.5 Å (atom-to-atom distances across opposite Cu and H (or *N*) atoms of ligands). Particularly, the distances between two opposite copper sites in each cavity of SMT-**1** and -**2** are 7.4 and 6.7 Å, respectively, suitable for the accommodation of one CO$_2$ molecule through the interaction of its two O atoms to the copper sites. Similarly, the reaction between H$_2$L$^2$ and Mo$_2$(O$_2$CCF$_3$)$_4$ afforded compound [Mo$_2$(L$^2$)$_2$(DMA)]$_2$·2DMA (**SMT-3**-DMA), with a similar
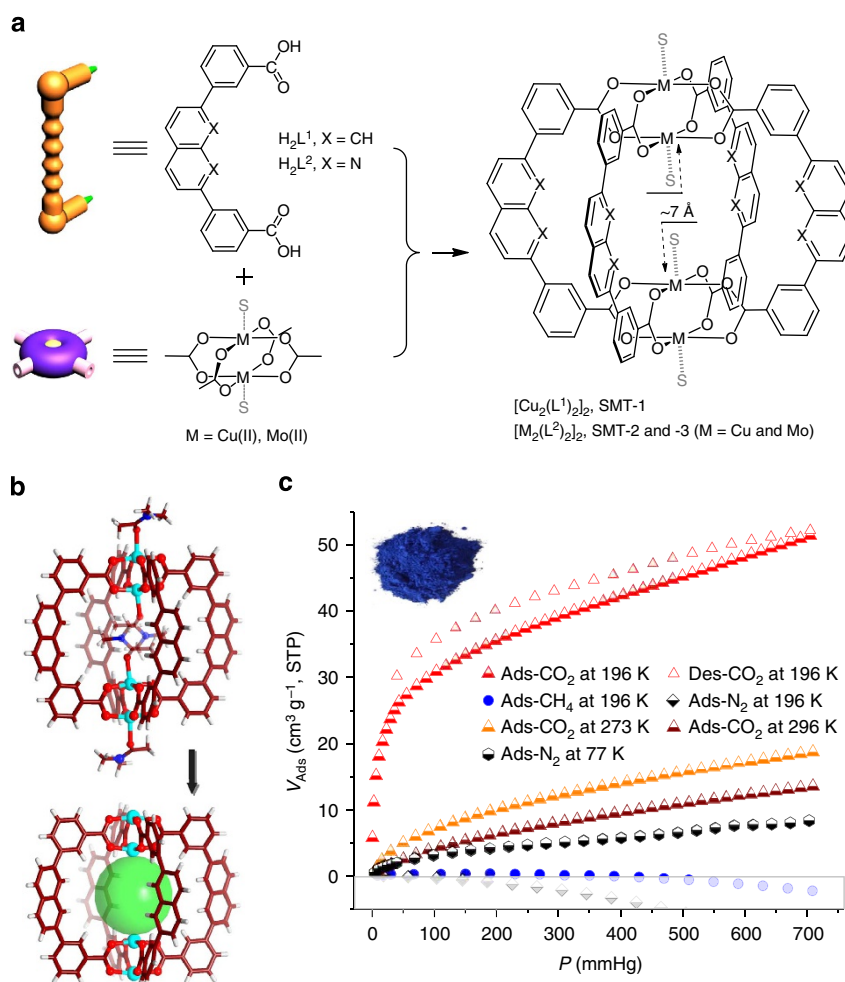


**Figure 2 | Synthesis, structures and CO$_2$ selective adsorption of precisely designed SMTs.** (**a**) Schematic representation of the construction of **SMT-1–3**: *S* is the coordinated solvent molecule, which can be removed through sample activation to yield an empty molecular cage for gas adsorption. (**b**) The molecular structure of **SMT-1** with (top) and without (bottom) coordinated solvent molecules. The colour schemes: Cu, cyan; O, red; N, blue; C, brown; and H, light grey. The green sphere represents the free space inside the molecular cage. (**c**) Gas adsorption isotherms of **SMT-1**, showing selective adsorption of CO$_2$ over CH$_4$ and N$_2$ (inset: a picture of activated **SMT-1** sample).

structure to that of **SMT-2**-DMA (see Supplementary Fig. S15). The size of the molecule and dimensions of the cavity are $11.5 \times 20.3$ and $7.3 \times 12.9$ Å, respectively.

The methanol-exchanged **SMT-1**-DMA was further activated under a vacuum at 80 °C to give desolvated material, **SMT-1**, which, as a representative of these SMTs, was tested for gas adsorption. As shown in Fig. 2c, **SMT-1** shows a significant adsorption for $CO_2$ at both low and enhanced temperatures, but almost excludes $N_2$ and $CH_4$. At 196 K and 1 atm, the uptake of $CO_2$ is 52 $cm^3 g^{-1}$ (2.32 mmol $g^{-1}$), corresponding to about 4 $CO_2$ molecules adsorbed per **SMT-1** molecule, implying that besides the cavities of SMT molecules, the space between them are also accessible for $CO_2$ adsorption. The evaluated Langmuir surface area is 153.7 $m^2 g^{-1}$ and the pore volume is 0.097 $cm^3 g^{-1}$, based on the $CO_2$ adsorption data at 196 K. The adsorption capacity of $CO_2$ at 273 and 296 K are 19 (0.85) and 14 (0.63) $cm^3 g^{-1}$ (mmol $g^{-1}$), corresponding to about 1.5 and 1 $CO_2$ molecules per **SMT-1**, respectively. The $CO_2$ adsorption enthalpy at zero coverage is ca. $-35$ kJ $mol^{-1}$ (see Supplementary Fig. S17), higher than that in most MOFs, particularly those constructed from pure carboxylate ligands and similar paddlewheel dicopper clusters[5,38]. However, at 196 K and higher temperatures, the adsorption of $N_2$ and $CH_4$ falls below the detection limit of our instrument. The lack of accurate data sets for $N_2$ and $CH_4$ adsorption limits the quantitative estimation of adsorption selectivities of these gases in this porous molecular material. It should also be pointed out that the desolvated **SMT-1** sample is still crystalline, as confirmed by PXRD (Supplementary Fig. S1), but the diffraction peaks deviate from those of fresh **SMT-1**-DMA due to the axial ligand removal and the resulting overall parking structure distortion. This observation differs from those of several previously reported MOP materials, which usually became amorphous after the solvent molecules were removed, but are still porous at the molecular level[7,37]. In addition, **SMT-2** also adsorbs $CO_2$ up to 25 $cm^3 g^{-1}$ (1.11 mmol $g^{-1}$) at 273 K, but the uptakes of $N_2$ and $CH_4$ are well below the detection limit (see Supplementary Fig. S18). It is clear that these precisely designed SMTs are efficient for the selective $CO_2$ adsorption.

To evaluate whether the $CO_2$ molecule prefers staying in the cavity of these SMTs, the $CO_2$-binding energy of the SMTs with a variety of proposed metal sites (Zn, Cu, Rh and Mo) was calculated using density functional theory (DFT). The simulation indicates that it is indeed energetically favourable for a $CO_2$ molecule to stay in the cavity of these SMTs (see Supplementary Table S9). Moreover, SMTs with different metal ions show distinct affinities towards $CO_2$. Among them, the Zn-based SMT shows the strongest interaction with a trapped $CO_2$ molecule, and the Mo-based one exhibits the weakest $CO_2$ affinity. These different $CO_2$ affinities arise from the ligand field preference of the metal ions. For example, the $Mo_2^{4+}$ cluster contains a quadruple bond and usually interacts weakly with axial ligands/guests[37]. The Zn-containing paddlewheel unit, on the other hand, contains no metal–metal bond. After removal of the coordinated solvent molecules, each $Zn^{2+}$ ion in the simulated compound prefers penta-coordination to square-pyramidal ligand environment through accepting an additional coordinating guest (such as $CO_2$), or to transfer to a tetrahedral environment. Because of the instability of square planar $Zn^{2+}$, it is difficult to synthesise robust Zn-based SMTs, or other MOFs built from Zn-based paddlewheel units.

The overall valid porosity of a MOP in the bulk sample is usually discounted because of the partial conglomeration of individual cages. When incorporated into a rigid porous framework, much more internal surface of MOP cages should become accessible.

**Building the pre-designed SMTs into extended materials.** Success in the construction of SMTs and their efficient capture of $CO_2$ molecules motivated us to build these molecular cages into extended framework materials to fully expose their internal surface and efficiently enhance the mass transfer for $CO_2$ adsorption and separation. The two above-mentioned strategies shown in Fig. 1 were tried initially, but only one, introducing the SMTs as building units into a MOF, has thus far been achieved. Incorporating these SMTs into other porous materials was hampered by the poor solubility of them in all tested solvents. To avoid precipitation of the SMT intermediate, we designed a ligand with two types of carboxylate groups, one to support the SMT and the other for the formation of an extended framework. Thus, an extended framework with SMTs can be assembled in a one-pot reaction. In this context, the dicarboxylic acid ligand $H_2L^1$ was functionalised by adding two additional carboxylic acid groups to generate 5,5′-(naphthalene-2,7-diyl)diisophthalic acid ($H_4L^3$, Fig 3a), which was synthesised by a procedure similar to that of $H_2L^1$, with diethyl 5-(4,4,5,5-tetramethyl-1,3,2-dioxaborolan-2-yl)isophthalate instead of 3-(methoxycarbonylphenyl)boronic acid. $H_4L^3$ reacted with $Cu(NO_3)_2 \cdot 2.5\ H_2O$ under solvothermal conditions (85 °C for 2 days) affording $[Cu(L^3)_{1/2}(S)]_n$ (**PCN-88**-S) (porous coordination network (PCN), S represents non-assignable solvent molecules), which has a 3D framework structure containing the pre-designed **SMT-1** units. The phase purity of the product was confirmed by PXRD (Supplementary Fig. S4) and the structure was analysed by single crystal X-ray diffraction (see Supplementary Information).

As shown in Fig. 3c, in **PCN-88**, there exist two conformers of $L^3$ ligands, one ($\alpha$-) with a dihedral angle of approximately 90° between the central and peripheral rings, whereas the other ($\beta$-) has a dihedral angle of approximately 0°, similar to a previously reported series[39]. In the MOF, four $\alpha$-$L^3$ ligands bridge two dicopper paddlewheel motifs to form a lantern-type unit similar to **SMT-1**, with eight additional carboxylate groups pointing to eight vertices of a quadrangular prism containing a SMT unit, in which the distance between two opposite copper sites in the cavity is about 7.4 Å (Fig 3b). Through these carboxylate groups, each quadrangular prism is linked to eight others by sharing eight dicopper motifs to form a 3D network (Fig 3a). In each end of a quadrangular prism, one of the four 'blades' of each of the four dicopper paddlewheel motifs are further capped by carboxylate groups of one $\beta$-$L^3$ ligand. On the other hand, only two types of supramolecular building units exist if the centres of all dicopper paddlewheel motifs are connected. One is shown in Fig. 3d, top, which is an elongated square dipyramid; the other is a concave elongated square dipyramid with the two pyramids inverted (Fig. 3d, bottom). The two units are complementary to each other in space filling. Six units of one type surround one unit of the other octahedrally forming a 3D network. After removal of coordinated solvent molecules, the solvent-accessible volume of the crystal (13667.3 Å$^3$ out of the 18544.0 Å$^3$ per unit cell) is 73.7% (ref. 40).

After activation of the as-synthesised material by successive methanol/dichloromethane solvent exchanges and heating at 100 °C under reduced pressure, **PCN-88** retained its crystallinity as confirmed by PXRD (Supplementary Fig. S4). $N_2$ and Ar adsorption isotherms at 77 and 87 K of the activated sample (see Supplementary Figs S19 and S21, respectively) further revealed permanent porosity. A two-step adsorption was observed in $N_2$ and Ar isotherms, with Brunauer-Emmett-Teller (BET) and Langmuir surface areas of 3308 and 3845 $m^2 g^{-1}$, respectively, based on the $N_2$ adsorption data (calculated from the first step of the adsorption isotherm). The stepwise adsorption isotherm can be explained by the existence of both meso- and micro-porous cages in the structure, as observed previously in
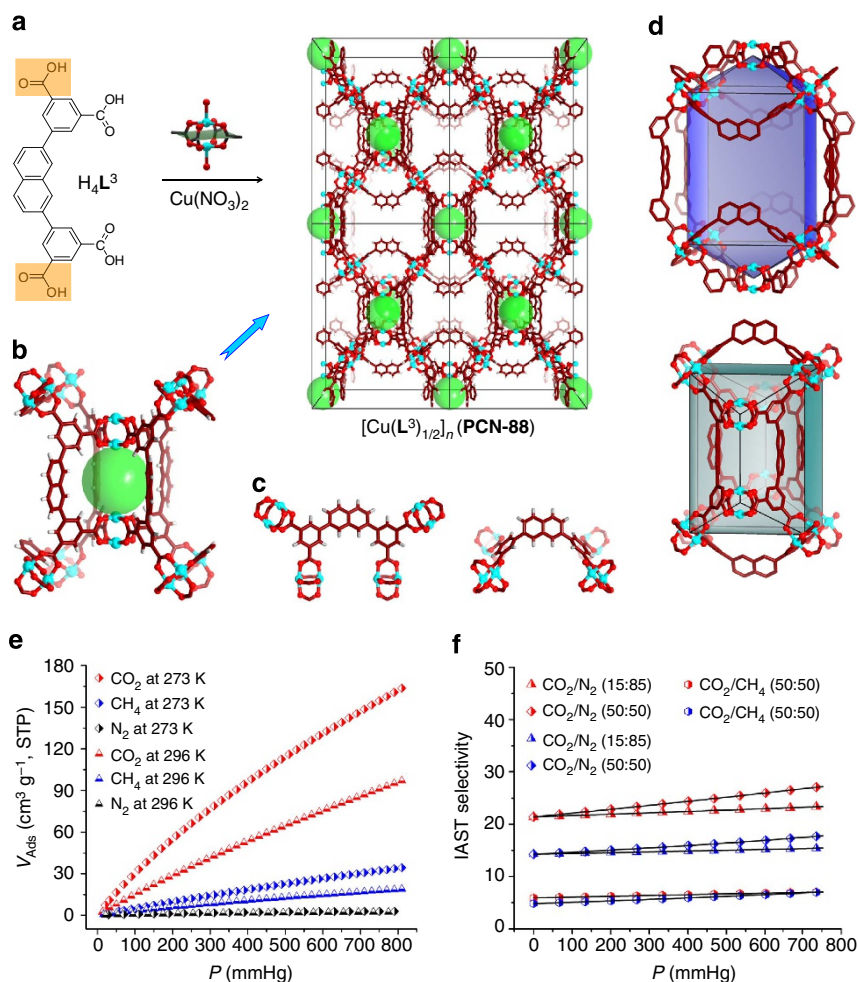
**Figure 3 | Construction, structure and selective gas adsorption performance of a MOF with built-in pre-designed SMTs. (a)** Schematic representation of the construction of **PCN-88** and its 3D framework structure. Colour scheme: Cu, cyan; O, red; C, brown; and H, light grey. The green sphere represents the free space inside the built-in SMTs. **(b)** A SMT unit in **PCN-88** with its linkages towards extending to the 3D framework. **(c)** Two conformers of ligand $L^3$ observed in **PCN-88**. **(d)** Two complementary polyhedra (elongated convex/concave square dipyramid) in **PCN-88** structure. Each polyhedron is formed by connecting dicopper nodes as vertices. **(e)** $CO_2$, $CH_4$ and $N_2$ adsorption isotherms of **PCN-88** at two temperatures. **(f)** Pressure-dependent IAST adsorption selectivities of $CO_2$ over $N_2$ and $CH_4$ at 273 K (red) and 296 K (blue) in **PCN-88** calculated based on single-component adsorption data.

similar systems[15]. As shown in Fig. 3e, **PCN-88** has a significant $CO_2$ (160 (7.14) and 94 (4.20) $cm^3 g^{-1}$ (mmol $g^{-1}$)) uptake, but little $CH_4$ (33 and 18 $cm^3 g^{-1}$) and $N_2$ uptake (2.6 and 2.1 $cm^3 g^{-1}$) at 273 and 296 K and 1 atm, respectively. It should be pointed out that the $CO_2$ uptake capacity of **PCN-88** at 296 K and 1 atm ranks among the highest for MOFs constructed from pure carboxylate ligands (see Supplementary Table S10) excluding the MOF-74 series, which are constructed from ligands with –OH moieties[5,38]. These observed selective adsorptions of $CO_2$ over $CH_4$ and $N_2$ can be attributed to the much stronger interactions of the $CO_2$ molecule with the adsorbent surface compared with those of the other two gases. The calculated Henry's law selectivities of $CO_2/CH_4$ and $CO_2/N_2$ are 7.3 and 67.9 at 273 K, and 5.3 and 18.1 at 296 K, respectively. Furthermore, ideal adsorbed solution theory (IAST (ref. 41) selectivities are also calculated by using the adsorption data of single-component gases (Fig. 3f). The values of IAST selectivities at 273 K and 1 bar for a 15/85 and a 50/50 $CO_2/N_2$ mixture are 23.1 and 27.4, respectively; and those at 296 K and 1 bar are 15.2 and 17.6, respectively. For a 50/50 $CO_2/CH_4$ mixture, corresponding values are 7.1 at 273 K and 7.0 at 296 K and

1 atm. The highly selective adsorption of $CO_2$ over $N_2$ and $CH_4$ suggests possible application of **PCN-88** in capturing $CO_2$ from flue gas or upgrading natural gas. The zero-coverage heat of adsorption of $CO_2$ in **PCN-88** is ca. $-27 kJ mol^{-1}$, which is higher than that in most MOFs constructed from pure carboxylate ligands and paddlewheel dicopper clusters[5,38]. This intermediate adsorption enthalpy implies a low-energy consumption for adsorbent regeneration, a desired property for separation applications. In fact, $CO_2$ capture in industry is highly process dependent, in which adsorbents are always optimised for a specific system. These equilibrium adsorption data only provide an initial step for improving the efficiency of a process. Additional experiments are still required for validating the practical value of these new adsorbents.
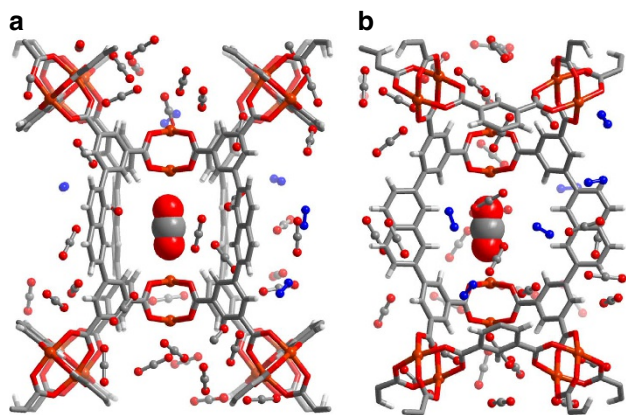
The $CO_2$, $CH_4$ and $N_2$ adsorption in **PCN-88** have also been evaluated by grand canonical Monte Carlo (GCMC) simulations. The simulated adsorption isotherms of single-component gases closely match the experimental ones as shown in Supplementary Fig. S36. To understand the adsorption behaviours of these gases in **PCN-88** at the molecular level, snapshots of the structures with adsorbed gas molecules at 296 K and 1 atm were analysed

(see Supplementary Fig. S37). It was found that the most preferred sites for $CO_2$ adsorption in **PCN-88** are the corner regions close to metal sites, probably because of the strong electrostatic interaction between them. On the contrary, $CH_4$ and $N_2$ molecules prefer to be adsorbed around the organic units because of van der Waals interactions. Furthermore, the adsorption behaviours and selectivities of gas mixture containing 15% $CO_2$ and 85% $N_2$ (mimicking real flue gas), as well as 50% $CO_2$ and 50% $CH_4$ in **PCN-88**, at different temperatures were also evaluated with GCMC simulations; the results are shown in Supplementary Figs S38–40. The evaluated adsorption selectivity of $CO_2$ over $N_2$ is about 15.3 and 10.2, and for $CO_2$ over $CH_4$ is 5.2 and 3.8 at 273 and 296 K and 1 atm, respectively. It is much more interesting that the snapshot at 296 K for the $CO_2/N_2$ mixture adsorption in **PCN-88** shows that there are quite a few $CO_2$ molecules but no $N_2$ molecules absorbed in the trap cavities. In some cases, the $CO_2$ molecule actually 'stands up' in the trap cavity, as shown in Fig. 4, demonstrating the validity of this designed SMT for $CO_2$ selective capture.

In addition, the diffusion of $CO_2$ and its mixture with $N_2$ in **PCN-88** at 296 K has also been studied by molecular dynamic simulations (see Supplementary Figs S43 and S44). It was found that single $CO_2$ molecules can diffuse into trap cavities but cannot be trapped at low loading; however, with increased loading, $CO_2$ is trapped in the cavities. For $CO_2/N_2$ mixtures, it was confirmed that only $CO_2$ molecules can be trapped in the cavities, which is consistent with the GCMC simulations discussed above. Again, this result shows that the pre-designed SMTs in **PCN-88** work well in selectively capturing $CO_2$ molecules.

**SMT's impact on $CO_2$ adsorption in PCN-88.** To further evaluate the effect of the SMTs on $CO_2$ adsorption in **PCN-88**, a control experiment was designed and performed. As shown in Fig. 5a,b, blocking the cavities of SMTs in **PCN-88** results in MOF $[Cu(L^3)_{1/2}(pyrazine)_{1/12}(S)]_n$ (**PCN-88′-S**), in which the trap cavities are occupied by pyrazine molecules by coordinating to two copper sites. **PCN-88′-S** was synthesised by a one-pot reaction of $H_4L^3$, pyrazine and $Cu(NO_3)_2 \cdot 2.5\ H_2O$ under conditions similar to that for **PCN-88-S**. Its structure is almost identical with that of **PCN-88-S** except for the blocked SMTs as
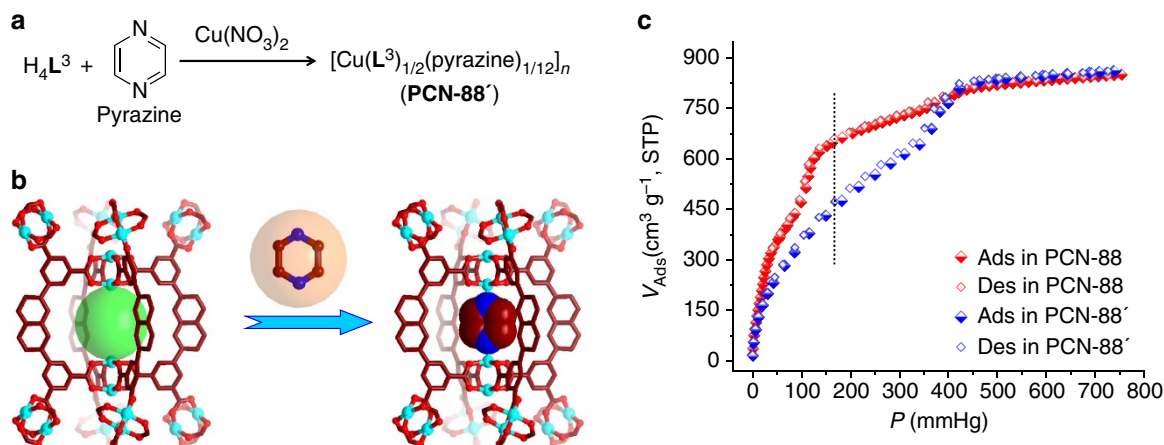
mentioned above. The structure contains a pore-accessible volume of 72.6% (13530.0 out of the 18646.0 $\text{Å}^3$ per unit cell volume) after removal of the coordinated solvent molecules[40]. The permanent porosity of desolvated material, **PCN-88′**, was revealed by the $N_2$ and Ar adsorption (see Supplementary Figs S20 and S22) at 77 and 87 K, respectively. The evaluated BET and Langmuir surface areas are 3042 and 3799 $\text{m}^2\,\text{g}^{-1}$, respectively, based on $N_2$ adsorption data. Similar to that of **PCN-88**, two-step adsorption isotherms for $N_2$ and Ar, and different adsorption quantities of $CO_2$ (119 (5.31) and 70 (3.13) $\text{cm}^3\,\text{g}^{-1}$ ($\text{mmol}\,\text{g}^{-1}$)), $CH_4$ (27 and 15 $\text{cm}^3\,\text{g}^{-1}$) and $N_2$ (2.4 and 1.8 $\text{cm}^3\,\text{g}^{-1}$) at 1 atm and 273 and 296 K, respectively, were observed (see Supplementary Fig. S31). Clearly, compared with **PCN-88**, **PCN-88′** yields a lower adsorption capacity towards these gases at 273 and 296 K due to the blocked SMT cavities. Interestingly at 195 K, both MOFs show almost the same $CO_2$ uptake capacities of about 850 $\text{cm}^3\,\text{g}^{-1}$ at 1 atm; however, **PCN-88** has a significantly enhanced $CO_2$ uptake compared with **PCN-88′** at pressures below 0.60 atm (450 mmHg), particularly at about 0.20 atm (150 mmHg) (Fig. 5c). This much higher adsorption at low pressure (lower than 150 mmHg) may be attributed to the contribution from SMTs in **PCN-88**, which is, as anticipated, very important for $CO_2$ separation from other gases, such as $N_2$ in flue gases, where the partial pressure of $CO_2$ is about 0.15 atm. For **PCN-88′**, the calculated Henry's law selectivities for $CO_2$ over $CH_4$ and $N_2$ are 6.1 and 49.4 at 273 K, and 5.0 and 12.6 at 296 K, respectively. Calculated IAST selectivities are 16.5 and 18.5 at 273 K and 1 bar, and 12.3 and 14.6 at 296 K, for 15/85 and 50/50 $CO_2/N_2$ mixtures, respectively. The related values for a 50/50 $CO_2/CH_4$ mixture are 6.6 and 5.8 at 273 and 296 K and 1 bar, respectively. All these evaluated selectivities in **PCN-88′** are lower than those in **PCN-88** (see Supplementary Table S6), indicating that the SMTs in the former have an effect on the selective adsorption of $CO_2$ over $CH_4$ and $N_2$. The zero-coverage heat of adsorption of $CO_2$ in **PCN-88′** is $-25\ \text{kJ}\,\text{mol}^{-1}$, again lower than that in **PCN-88**. In addition, it was also noted that **PCN-88** has a higher $H_2$ uptake than that of **PCN-88′** at 77 and 87 K, respectively, but both show similar adsorption enthalpies (see Supplementary Figs S24–26). In conclusion, this control experiment shows that the pre-designed SMTs in **PCN-88** have a significant influence on the adsorption of $CO_2$ in the low-pressure region.

**Discussion**

All results discussed above evidently demonstrate the feasibility of precisely designing a cavity in porous MOMs for specific adsorption-based applications. Clearly, designing a MOF or other composite with a higher density of SMTs will substantially improve the overall adsorption performance of a particular guest molecule, such as $CO_2$ in this SMT-based system presented here. For many years, there has been a push towards porous materials with high surface areas and large pore sizes, particularly for MOFs. But for $CO_2$ selective adsorption or capture (also for $H_2$ storage), these features have not been effective. Recently, a strategy based on pore space partition in a MOF through cage-within-cage, or core-shell, type architecture has been proposed by Bu and colleagues[42], as a strategy to optimise the pore space for better $CO_2$ capture. But the cage-within-cage configuration does not address the individual fit between the partitioned pore space and the size of the gas molecule. Here we represent the first time (to our knowledge) to design a cage-type assembly to specifically address the trapping of a particular molecule based on its chemical (polarity and so on) and physical (size and shape) properties. The advantage of this method is that it not only enhances the host–guest interactions because of an optimum fit,



**Figure 4 | Simulated locations of $CO_2$ and $N_2$ molecules in PCN-88 for $CO_2/N_2$ (15:85) mixture.** Simulation performed with a $CO_2/N_2$ (15:85) mixture at 296 K and 3 Mpa. Viewed from different directions: (**a**) along the crystallographic z direction and (**b**) along the x direction. Colour scheme: Cu, dark orange; O, red; N, blue; C, dark grey; and H, light grey. It is clear that one $CO_2$ molecule (shown in space-filling model) can be trapped in the centre of a SMT cavity.

**Figure 5 | Control experiment to identify the effect of SMTs in the PCN-88 on CO₂ adsorption.** (**a**) Schematic representation of the synthesis of **PCN-88′**. (**b**) Schematic representation of introducing a pyrazine molecule into the cavity of **PCN-88** to block the SMT. Colour scheme: Cu, cyan; O, red; and C, brown. The green sphere represents the free space inside the SMT. (**c**) CO₂ adsorption isotherms of **PCN-88** and -**88′** at 196 K, showing significantly different uptakes at low pressure due to the contribution of SMTs in the former.

but it also simultaneously endows the material with superior selectivity over other guest molecules because the cavity is custom-designed for a specific molecule.

In summary, a new concept, the 'SMT' has been utilised in designing porous materials at the molecular level for specific adsorption-based applications. As an experimental proof-of-concept, such a SMT was first designed and synthesised for $CO_2$ molecule capture by the precise selection of organic ligand and metal node to form a MOP. Experimental and computational simulation results demonstrate the efficiency of this MOP-based SMT in the preferential adsorption of $CO_2$ over $N_2$ and $CH_4$, which are important for $CO_2$ capture from flue gas and $CH_4$ upgrading. Building this SMT into a MOF with an extended framework structure was achieved, again, through ligand design. This resulting MOF preserves the SMT properties in capturing $CO_2$ molecules, therefore showing good performance in the selective adsorption of $CO_2$. In principle, by judiciously designing a SMT and thereby its extension into porous frameworks, this method can be applied in the synthesis of other new MOMs and composite materials for other specific applications, such as $H_2$ storage and even $CO_2$ activation by trapping one $CO_2$ in a confined cavity with strongly binding active sites. These materials may be used in applications such as small molecule capture, activation, conversion and storage, wherever binding single guest molecule is a prerequisite.

## Methods

**Materials and syntheses.** All general reagents and solvents (analytical grade (AR) grade) were commercially available and used as received. The protonated ligands 3,3′-(naphthalene-2,7-diyl)dibenzoic acid ($H_2L^1$), 3,3′-(1,8-naphthyridine-2,7-diyl)dibenzoic acid ($H_2L^2$), 5,5′-(naphthalene-2,7-diyl)diisophthalic acid ($H_4L^3$) and 5,5′-(1,8-naphthyridine-2,7-diyl)diisophthalic acid ($H_4L^4$, not used in the synthesis of MOFs because of its high cost) were newly designed and synthesised by using palladium-catalysed coupling reactions, followed by hydrolysis. The precursors in these reactions were purchased or synthesised according to the literature methods. **SMT-1**-DMA and **SMT-2**-DMA were synthesised by the reaction of $Cu_2(OAc)_4 \cdot 2H_2O$ with corresponding carboxylic acid ligands in DMA at room temperature. Single crystals of **SMT-1**-DMA were obtained by layering a solution of $H_2L^1$ in DMA upon a DMA solution of $Cu_2(OAc)_4 \cdot 2H_2O$ and staying for several days. For **SMT-2**-DMA, two solutions of $H_2L^2$ and $Cu_2(OAc)_4 \cdot 2H_2O$ in DMA were mixed and left undisturbed for several days to obtain crystals. Single crystals of **SMT-3**-DMA were synthesised by heating a DMA solution of $H_2L^2$ and $Mo_2(O_2CCF_3)_4$ with 48% aqueous solution of $HBF_4$ at 85 °C for 12 h. These SMT-DMA crystals slowly lose transparency as solvent molecules evaporate into the air over a longer period of time, and are insoluble in DMA, N,N-dimethylformamide, dimethyl sulfoxide, methanol and acetone. **PCN-88**-*S* and -**88′**-*S* were synthesised by similar solvothermal procedures: a DMA/water solution containing $Cu(NO_3)_2 \cdot 2.5H_2O$, $H_4L^3$; a few drops of $HBF_4$ solution (and pyrazine for **PCN-88′**-*S*) was heated at 85 °C for 2 days to afford single crystals. Phase purity of all products was evaluated by PXRD; general characterisation including infrared and thermogravimetric analysis were carried out. Detailed descriptions of syntheses and characterisation are given in the Supplementary Methods.

**X-ray single-crystal diffraction.** Data were collected on a Bruker AXS APEX-II CCD (charge-coupled device) diffractometer with a fine-focus sealed-tube X-ray source (Mo-$K_\alpha$) and the structures were solved by direct methods. Details are provided in the Supplementary Information. In all the structures except **SMT-3**-DMA, free solvent molecules are disordered, and attempts to locate and refine all the solvent molecule peaks were unsuccessful. Diffused electron densities resulting from these solvent molecules (except the O atoms of coordinated solvents) were removed from the data set using the SQUEEZE routine of PLATON and refined further using the data generated[40]. The coordinated solvent molecules in **PCN-88**-*S* and -**88′**-*S* are also disordered, only the O atoms were left and refined and other atoms were omitted. Contents of the removed solvent region are not represented in the unit cell contents in the crystal data of related compounds. Attempts to determine the final formula of these compounds from the SQUEEZE results, combined with elemental analysis and thermogravimetric analysis data, were unsuccessful because of the volatility of crystallisation solvents during measurements.

**Gas adsorption.** Gas adsorption measurements were performed using an ASAP 2020 volumetric adsorption analyser. A high-purity grade (99.999%) of gases was used throughout the adsorption experiments. Before adsorption, the sample was activated by solvent exchange (in several cycles using fresh methanol) to remove the coordinated DMA molecules, followed by degassing at elevated temperature and vacuum. Details are given in the Supplementary Information. To get more precise adsorption data, particularly for $N_2$ and $CH_4$ adsorption at higher temperatures, such as 296 K, the free space of the sample holder was minimised as much as possible. In evaluating the adsorption selectivities of these material towards different gases including $CO_2$, $N_2$ and $CH_4$, Henry's law selectivity and IAST selectivity are calculated based on the adsorption data of each single gas.

**Computational simulations.** DFT calculations were performed for three purposes: to optimise the geometries of $CO_2$ interaction with SMTs; to evaluate the binding energies between $CO_2$ and SMTs; and to calculate the partial charges of **PCN-88** framework atoms that were used in GCMC simulations. All DFT calculations were carried out using Gaussian 09[43]. GCMC simulations were employed to calculate the uptake of single gases and gas mixtures in **PCN-88**, which was treated as a rigid framework, using the MUSIC program[44]. The potential parameters for the framework atoms were taken from DREIDING force field. Molecular dynamic simulations were performed using the DL-POLY-2.20 with the Berendsen thermostat in the NVT ensemble. Detailed descriptions and additional discussions are provided in the Supplementary Methods.

## References

1. Keith, D. W. Why Capture CO₂ from the atmosphere? *Science* **325,** 1654–1655 (2009).
2. Kramer, G. J. & Haigh, M. No quick switch to low-carbon energy. *Nature* **462,** 568–569 (2009).
3. Rochelle, G. T. Amine scrubbing for CO₂ capture. *Science* **325,** 1652–1654 (2009).
4. Choi, S., Drese, J. H. & Jones, C. W. Adsorbent materials for carbon dioxide capture from large anthropogenic point sources. *ChemSusChem* **2,** 796–854 (2009).
5. Sumida, K. *et al.* Carbon dioxide capture in metal–organic frameworks. *Chem. Rev.* **112,** 724–781 (2012).
6. Li, J.-R., Sculley, J. & Zhou, H.-C. Metal-organic frameworks for separations. *Chem. Rev.* **112,** 869–932 (2012).
7. Li, J.-R. & Zhou, H.-C. Bridging-ligand-substitution strategy for the preparation of metal-organic polyhedra. *Nat. Chem.* **2,** 893–898 (2010).
8. Seo, J. S. *et al.* A homochiral metal-organic porous material for enantioselective separation and catalysis. *Nature* **404,** 982–986 (2000).
9. Kosal, M. E., Chou, J.-H., Wilson, S. R. & Suslick, K. S. A functional zeolite analogue assembled from metalloporphyrins. *Nat. Mater.* **1,** 118–121 (2002).
10. Matsuda, R. *et al.* Highly controlled acetylene accommodation in a metal-organic microporous material. *Nature* **436,** 238–241 (2005).
11. Hurd, J. A. *et al.* Anhydrous proton conduction at 150 °C in a crystalline metal-organic framework. *Nat. Chem.* **1,** 705–710 (2009).
12. Xiao, B. *et al.* Chemically blockable transformation and ultraselective low-pressure gas adsorption in a non-porous metal organic framework *Nat. Chem.* **1,** 289–294 (2009).
13. Clever, G. H., Tashiro, S. & Shionoya, M. Inclusion of snionic guests inside a molecular cage with palladium(II) centers as electrostatic anchors. *Angew. Chem. Int. Ed. Engl.* **48,** 7010–7012 (2009).
14. Kawamichi, T., Haneda, T., Kawano, M. & Fujita, M. X-ray observation of a transient hemiaminal trapped in a porous network. *Nature* **461,** 633–635 (2009).
15. Farha, O. K., Yazaydın, A. Ö., Eryazici, I., Malliakas, C. D., Hauser, B. G. & Kanatzidis, M. G. *et al. De novo* synthesis of a metal-organic framework material featuring ultrahigh surface area and gas storage capacities. *Nat. Chem.* **2,** 944–948 (2010).
16. Rabone, J. *et al.* An adaptable peptide-based porous material. *Science* **329,** 1053–1057 (2010).
17. Vaidhyanathan, R. *et al.* Direct observation and quantification of CO₂ binding within an amine-functionalized nanoporous solid. *Science* **330,** 650–653 (2010).
18. Blake, A. J. *et al.* Photoreactivity examined through incorporation in metal-organic frameworks. *Nat. Chem.* **2,** 688–694 (2010).
19. Horcajada, P. *et al.* Porous metal-organic-framework nanoscale carriers as a potential platform for drug delivery and imaging. *Nat. Mater.* **9,** 172–178 (2010).
20. Gascon, J. & Kapteijn, F. Metal-organic framework membranes—high potential, bright future? *Angew. Chem. Int. Ed. Engl.* **49,** 1530–1532 (2010).
21. An, J. *et al.* Metal-adeninate vertices for the construction of an exceptionally porous metal-organic framework. *Nat. Commun.* **3,** 604 (2012).
22. Zhang, Y.-B. *et al.* Geometry analysis and systematic synthesis of highly porous isoreticular frameworks with a unique topology. *Nat. Commun.* **3,** 642 (2012).
23. Bloch, E. D. *et al.* Hydrocarbon separations in a metal-organic framework with open iron(II) coordination sites. *Science* **335,** 1606–1610 (2012).
24. Suh, M. P., Park, H. J., Prasad, T. K. & Lim, D.-W. Hydrogen storage in metal-organic frameworks. *Chem. Rev.* **112,** 782–835 (2012).
25. Eddaoudi, M. *et al.* Systematic design of pore size and functionality in isoreticular MOFs and their application in methane storage. *Science* **295,** 469–472 (2002).
26. Perry, J. J., Perman, J. A. & Zaworotko, M. J. Design and synthesis of metal-organic frameworks using metal-organic polyhedra as supermolecular building blocks. *Chem. Soc. Rev.* **38,** 1400–1417 (2009).
27. O'Keeffe, M. Design of MOFs and intellectual content in reticular chemistry: a personal view. *Chem. Soc. Rev.* **38,** 1215–1217 (2009).
28. Ma, L., Falkowski, J. M., Abney, C. & Lin, W. A series of isoreticular chiral metal-organic frameworks as a tunable platform for asymmetric catalysis. *Nat. Chem.* **2,** 838–846 (2010).
29. Morris, R. E. & Bu, X. Induction of chiral porous solids containing only achiral building blocks. *Nat. Chem.* **2,** 353–361 (2010).
30. Zhao, D., Timmons, D. J., Yuan, D. & Zhou, H.-C. Tuning the topology and functionality of metal-organic frameworks by ligand design. *Acc. Chem. Res.* **44,** 123–133 (2010).
31. Henke, S. & Fischer, R. A. Gated channels in a honeycomb-like zinc – dicarboxylate – bipyridine framework with flexible alkyl ether side chains. *J. Am. Chem. Soc.* **133,** 2064–2067 (2011).
32. Xiang, S.-C. *et al.* Rationally tuned micropores within enantiopure metal-organic frameworks for highly selective separation of acetylene and ethylene. *Nat. Commun.* **2,** 204 (2011).
33. Wilmer, C. E. *et al.* Large-scale screening of hypothetical metal-organic frameworks. *Nat. Chem.* **4,** 83–89 (2012).
34. Otsubo, K. *et al.* Bottom-up realization of a porous metal–organic nanotubular assembly. *Nat. Mater.* **10,** 291–295 (2011).
35. Vukotic, V. N., Harris, K. J., Zhu, K., Schurko, R. W. & Loeb, S. J. Metal-organic frameworks with dynamic interlocked components. *Nat. Chem.* **4,** 456–460 (2012).
36. Cohen, S. M. Postsynthetic methods for the functionalization of metal-organic frameworks. *Chem. Rev.* **112,** 970–1000 (2012).
37. Li, J.-R. *et al.* Ligand bridging-angle-driven assembly of molecular architectures based on quadruply bonded Mo – Mo dimers. *J. Am. Chem. Soc.* **132,** 17599–17610 (2010).
38. Li, J.-R. *et al.* Carbon dioxide capture-related gas adsorption and separation in metal-organic frameworks. *Coord. Chem. Rev.* **255,** 1791–1823 (2011).
39. Sun, D., Ke, Y., Mattox, T. M., Ooro, B. A. & Zhou, H.-C. Temperature-dependent supramolecular stereoisomerism in porous copper coordination networks based on a designed carboxylate ligand. *Chem. Commun.* 5447–5449 (2005).
40. Spek, A. L. Single-crystal structure validation with the program PLATON. *J. Appl. Crystallogr.* **36,** 7–13 (2003).
41. Myers, A. L. & Prausnitz, J. M. Thermodynamics of mixed-gas adsorption. *AIChE J.* **11,** 121–127 (1965).
42. Zheng, S.-T. *et al.* Pore space partition and charge separation in cage-within-cage indium-organic frameworks with high CO₂ uptake. *J. Am. Chem. Soc.* **132,** 17062–17064 (2010).
43. Frisch, M. J. *et al. GAUSSIAN 09 Program* (Gaussian, Inc., Wallingford, CT, 2009).
44. Gupta, A., Chempath, S., Sanborn, M. J., Clark, L. A. & Snurr, R. Q. Object-oriented programming paradigms for molecular modeling. *Mol. Simul.* **29,** 29–46 (2003).

## Acknowledgements

## Author contributions

J.R.L. and H.-C.Z. conceived and designed the experiments and co-wrote the paper. J.R.L. performed most of experiments and analysed data. J.Y. worked on all computational simulations under the guidance of P.B.B. W.L. performed ligand synthesis, and L.B.S. and J.S. performed the measurement of gas adsorption. All authors discussed the results and commented on the manuscript.

## Additional information